Int. J. Heat Mass Transfer. Vol. 17, pp. 293–306. Pergamon Press 1974. Printed in Great Britain

THE TURBULENT BOUNDARY LAYER WITH FOREIGN GAS INJECTION—II. PREDICTIONS AND MEASUREMENTS IN SEVERE STREAMWISE PRESSURE GRADIENTS

R. J. BAKER and B. E. LAUNDER
Mechanical Engineering Dept., Imperial College, Exhibition Road, London S.W.7, England

(*Received* 28 *February* 1973 *and in revised form* 8 *August* 1973)

Abstract—The paper proposes a new and simple version of the Prandtl mixing length hypothesis for flow past smooth surfaces. The model has been used in obtaining extensive predictions of boundary layers on porous surfaces including flows with steep density and pressure gradients measured in the present study. Very good agreement of predictions with measurements is obtained except in flows in adverse pressure gradients and under conditions of high blowing. In these cases, because of convective transport of turbulence, the level of mixing length in the outer part of the boundary layer does not increase as fast as the boundary-layer thickness.

NOMENCLATURE

A^+, Van Driest sublayer function (taken as constant 26);
C_f, Coefficient of friction $\equiv 2\tau_w/\rho_G u_G^2$;
h, stagnation enthalpy;
H_{12}, shape factor $\equiv \delta_1/\delta_2$;
k, mixing length constant;
K, acceleration parameter $\equiv \nu_G/u_G^2\, du_G/dx$;
l, mixing length;
M, mass-transfer parameter $\equiv \dot{m}''s/\rho_G u_G$;
m, mass-fraction;
$\dot{m}_w''$, mass-transfer rate at the surface (per unit area);
P, streamwise pressure gradient;
P^+, normalised pressure gradient, $u/\rho^{\frac{1}{2}}\tau_w^{\frac{3}{2}}\, dp/dx$;
R_{max}, turbulent Reynolds number, $\sqrt{(\tau_{max}/\rho)}\, y_G/\nu$;
R_2, momentum Reynolds number, $\rho u\delta_2/\mu$;
St, Stanton number, $J_{\phi,w}/\rho_G u_G(\phi_w - \phi_G)$;
u, streamwise velocity;
V, normal velocity;
V^+, normalized cross-stream velocity, $V/\sqrt{(\tau_w/\rho)}$;
x, streamwise distance;
y, cross-stream distance;
y^+, normalized cross-stream distance, $y/\nu\sqrt{(\tau_w/\rho)}$;
δ_1, displacement thickness,

$$\int_0^\infty \left(1 - \frac{\rho u}{\rho_G u_G}\right) dy;$$

δ_2, momentum thickness,

$$\int_0^\infty \left(1 - \frac{u}{u_G}\right)\frac{\rho u}{\rho_G u_G}\, dy;$$

δ_{2m}, concentration momentum thickness,

$$\int_0^\infty \left(\frac{m - m_G}{m_w - m_G}\right)\frac{\rho u}{\rho_G u_G}\, dy;$$

λ, mixing length constant;
μ, laminar viscosity;
ν, kinemtatic viscosity;
$\sigma_{\phi,t}$, turbulent Prandtl or Schmidt numbers;
ρ, density;
τ, shear-stress;
ϕ, refers to either normalized mass fraction or enthalpy.

Subscripts

A, air;
F, freon;
G, at the free stream;
t, turbulent;
w, at the wall.

1. INTRODUCTION

THE BEHAVIOUR of turbulent boundary layers with foreign gas injection is the subject of considerable current interest. The interest stems in part from the recognition that transpiration cooling provides a very effective process for protecting surfaces exposed to high-temperature flows. There is interest too because of the fundamental light these flows may shed on turbulent mixing processes: it is a flow where one may easily establish large density gradients across the flow and the shear-stress profile with strong injection will be very much modified from that found on a flat impermeable plate.

A companion paper [1] has provided experimental

data on the development of turbulent boundary layers in zero pressure under various levels of freon-12 injection. In the context of the above paragraph, these data provided 'fundamental' information about the flow structure. To complement that study, in the present work our objective has been to consider a range of external pressure distributions more akin to those that might be encountered in actual transpiration–cooling configurations. The apparatus and experimental technique employed were the same as that described in [1]; here the pressure gradients were achieved by modifying the roof of the test section as indicated in Fig. 1.

The paper presents predictions of the new experimental data and of other transpired flows based on a mixing-length model of turbulence transport.

While a number of turbulence models (e.g. [3–5]) possess a greater width of applicability, the mixing length hypothesis has proved to be very successful for the prediction of wall-boundary layers; and because of its simplicity, it is very economical of computer time.*

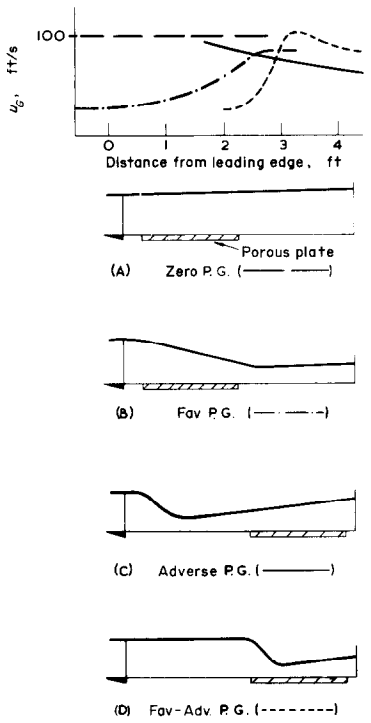

FIG. 1. Test section configurations for various pressure gradients.

* For example, with the mixing length hypothesis a typical finite-difference solution requires only 30 per cent of the computer time needed when the 2-equation turbulence model of [4] is employed.

Among the papers dealing with the prediction of uniform property transpired boundary layers with versions of the mixing length hypothesis are those of Powell and Strong [6] Cebici and Mosinskis [7], Kays, Moffat and Thielbahr [8] and Kays [9]. The last of these presents the most refined form of the model, being based on the vast amount of experimental data obtained by Professor Kays' group over the past decade. This version of predicting quite accurately even strongly non-equilibrium flows where virtually step changes occur in the local level of transpiration or pressure gradient. Nevertheless, the great deal of empirical correlation that has gone into this model seems to weaken its prospect of giving good predictions in flows of a different kind from those from which it has been derived. Our own approach had been to keep the number of empirical inputs to a minimum. The model adopted and the rationale for its choice are presented below.

2. THE MODEL OF TURBULENCE

According to the mixing-length hypothesis, the turbulent fluxes of momentum, enthalpy and species across the boundary layer are linked to the corresponding mean-quantity profiles by the relations

$$-\rho\overline{u'v'} = \mu_t \frac{\partial u}{\partial y}$$

$$-\rho\overline{h'v'} = \frac{\mu_t}{\sigma_{h,t}} \frac{\partial h}{\partial y} \tag{1}$$

$$-\rho\overline{m'v'} = \frac{\mu_t}{\sigma_{m,t}} \frac{\partial_m}{\partial y}$$

where

$$\mu_t = \rho l^2 \left| \frac{\partial u}{\partial y} \right| \tag{2}$$

and l is the so-called mixing length. To complete the model we must prescribe the distribution across the boundary layer of l and of the turbulent Prandtl and Schmidt numbers, $\sigma_{h,t}$ and $\sigma_{m,t}$; we consider the former first.

Escudier [10] has shown that, excluding the zone in the immediate neighbourhood of the wall, the distribution of mixing length across boundary layers on impermeable surfaces is well represented by the ramp function.

$$l = ky \qquad 0 < y \leqslant \lambda y_G/k \tag{3a}$$

$$l = \lambda y_G \qquad \frac{\lambda y_G}{k} < y \leqslant y_G. \tag{3b}$$

[1] has shown that the same basic distribution

occurs in transpired boundary layers too, even when steep density gradients are present. The slope of the ramp, k, emerged from this survey as a constant, independent of mass injection rate, density gradient or Reynolds number. No evidence was found of an increase in k above its asymptotic value for values of R_2 less than 6000 reported by Simpson [11]. For the present computations it is therefore assumed that:

$$k = 0{\cdot}425 \tag{4}$$

a value which fits the data of [1] very accurately. Other workers have adopted values between 0·40 and 0·44; so the present choice is a consensus of current practice.

Escudier found that the value of λ, while exhibiting scatter from one flow to another, displayed no consistent trends; he therefore recommended a constant value of 0·07. Reference [1], which confined attention to transpired flows wlthout streamwise pressure gradient, showed a systematic decrease of λ with distance along the plate, with increase of injection rate and with increase of density ratio between injectant and primary fluid. All these effects could be accounted for quite well by assuming λ to be a unique function of the Reynolds number R_{max}, the formula:

$$\lambda = 0{\cdot}075(1 + \exp - R_{max}/400) \tag{5}$$

providing a reasonable fit to the data; it is this version which is used in the present computations except where specifically stated to the contrary.

It appears somewhat strange that λ should display a dependence on viscosity when k does not, since the turbulence Reynolds number in the outer region is much larger than near the wall. The effect is well established however: Kays *et al.* [8] proposed that λ should vary as $R_2^{-0{\cdot}125}$ for low Reynolds number and Coles [12] has shown that the strength of the "wake" for unblown boundary layers does not become fully established until R_2 has reached about 5000.

In the immediate vicinity of the surface viscous action reduces the level of mixing length below the value implied by equation (3a). Thus we write:

$$l = kyD \tag{6}$$

where the damping function D increases from zero at the wall to unity in the fully turbulent region. Most proposals for D have been based upon extensions of Van Driest's damping function, often expressible in the form

$$D = 1 - \exp - [y^+(\sqrt{\tau^+})/A^+]. \tag{7}$$

Patankar and Spalding [14a] assumed A^+ to take the constant value of 26 proposed by Van Driest. Several independent studies soon showed, however that equation (7) gave too large values of l in strongly accelerated flows and too small values in blown boundary layers; as a result wall friction and heat-transfer predictions were commonly in error by 50 per cent or more. In an attempt to remedy this deficiency A^+ was held to depend on the local levels of the dimensionless pressure gradient and mass transfer, p^+ and v_w^+, perhaps the most recent proposal of this kind being that of Kays [9]. Even this degree of elaboration brought satisfactory predictions of Stanton number only where v_w^+ and p^+ changed slowly in the streamwise direction. In strongly non-equilibrium flows therefore Kays recommends the use of an empirical equation which relates the streamwise rate of change of A^+ to the amount that A^+ differs from its equilibrium value.*

In considering the form of D for the present work, we concluded that the approaches outlined above were not attractive. The empirical functions proposed were already elaborate; and these had been devised only with reference to uniform property flows. A form that would suffice for flows with appreciable gradients of ρ and μ would doubtless need to be even more intricate.

It seemed preferable therefore to seek a *single*, more fundamental agency to which changes in A^+ associated with both pressure gradient and mass transfer could be attributed. The variation of shear stress in the vicinity of a wall seemed to provide such a unifying parameter.

As a simplification of the proposals of [16] some preliminary computations were made in which A^+ was found from the formula:

$$A^+ = 26/\tau^+ \qquad y^+ = A^+.$$

Evidently, for sucked and accelerated flows where the shear stress falls with distance from the wall, A^+ takes on values greater than 26; likewise for blown and retarded flow A^+ is smaller than in the case of a flat plate boundary layer. The implied effects on A^+ were of the right sign and of about the correct magnitude for near-equilibrium sucked and accelerated boundary layers.†

There was a further advantage which accrued from using the stress profile to determine A^+ The shear stress distribution within the fluid does not alter immediately as a result of a suddenly imposed pressure

* The practice had been earlier proposed and tested with moderate success by Jones and Launder [15].

† A recent report by Anderson *et al.* [17] adopts a very similar form except that the shear stress ratio is evaluated at $3A^+$ rather than A^+. Agreement with experiment was excellent for the limited range of flows considered.

gradient, i.e. *the stress profile lags behind the local variation of* p^+. It thus became possible to discard the ad hoc 'lag equation' for A^+ which had been found necessary with earlier studies.

The preliminary computations showed however that the above formula for A^+ was rather prone to numerical instability. The following similar but even simpler damping function was therefore adopted:

$$D = 1 - \exp - y^+\tau^+/26 \tag{8}$$

a form which was free from this problem. Notice that this final form differs from the proposal of [14] and others only in the exponent of τ^+. Equations (7) and (8) therefore give simply the same results in near equilibrium flows where the change in τ across the sublayer is slight; however, when shear stress gradients normal to the surface are large, equation (8) is decisively better than (7).

Turbulent Prandtl/Schmidt number

The value of the turbulent Prandtl/Schmidt number, $\sigma_{\phi,t}$, determined from experiment is inherently an imprecise one. This fact almost certainly accounts for the considerable scatter in the reported data. Given this spread, however, heat and mass transfer data suggest that $\sigma_{\phi,t}$ is close to unity near the surface, falling gradually to about 0·5 near the edge of the flow.

A number of data [1, 18, 19] suggest a sharp rise in $\sigma_{\phi,t}$ very near the wall; in this region however turbulence levels are high and probably affect the measured velocity profile in a non-random way. Perhaps the best reason for treating the Prandtl/Schmidt number as constant in the near-wall region is Patankar and Spalding's [14] finding that this supposition gives accurate prediction of mass transfer rates in pipes at high Schmidt numbers. We made a number of calculations with a constant value of $\sigma_{\phi,t}$ of 0·9 and found this led to entirely acceptable predictions of concentration profiles except for extreme levels of freon injection; but because of this defect it was decided to adopt Rotta's [20] proposal which fitted the data of [1] and [18] well:

$$\sigma_{\phi,t} = 0{\cdot}95 - 0{\cdot}45(y/y_G)^2. \tag{9}$$

Solutions of the equations

The steady, 2-dimensional mean-flow transport equations for momentum and a conserved property ϕ such as enthalpy of chemical species may be written:

$$\rho u\frac{\partial u}{\partial x} + \rho v\frac{\partial u}{\partial y} = -\frac{\mathrm{d}p}{\mathrm{d}x} + \frac{\partial}{\partial y}\left[(\mu_t + \mu)\frac{\partial u}{\partial y}\right] \tag{10}$$

$$\rho u\frac{\partial \phi}{\mathrm{d}x} + \rho v\frac{\partial \phi}{\partial y} = \frac{\partial}{\partial y}\left[\left(\frac{\mu_t}{\sigma_{\phi,t}} + \frac{\mu}{\sigma_\phi}\right)\frac{\partial \phi}{\partial y}\right] \tag{11}$$

Equations (10) and (11), with the turbulence model defined by equations (2)–(9) incorporated, have been solved by means of the Patankar–Spalding [14b] finite-difference procedure for parabolic equations. Typically 40 cross-stream nodes were used to cover the boundary layer, the spacing being non-uniform with about 50 per cent of the nodes in the region $y^+ < 100$. The nearest grid point to the wall was always located in the viscous sublayer where turbulent transport was negligible. Computing time on a CDC 6600 computer was about 10s per run.

We could find no experimental data of the molecular transport coefficients for freon/air mixtures. For the flows with freon injection, we therefore determined μ and σ_ϕ as described in Appendix 1.

3. PRESENTATION AND DISCUSSION OF RESULTS

In the predictions presented below the variation of the boundary layer shape factor, H_{12}, and skin friction coefficient provide the main basis for assessing the satisfactoriness or otherwise of the calculated behaviour. In the past it has been customary to draw comparison also with the variation of R_2. For blown boundary layers, however, wall friction is such a small contributor to the growth of the boundary layer that agreement with experiment of the momentum thickness Reynolds number shows little more than that the experimental data are two dimensional. For all except one of the test cases considered here measured and predicted variation of R_2 are scarcely distinguishable; we therefore omit the comparison for all but the exceptional case.

The first flow considered (in Figs. 2 and 3) is the flat plate boundary layer with uniform air injection, the data being those of McQuaid [21], Simpson *et al.* [22] and the authors [1]. The turbulence model chosen took particular note of experimental data of this particular flow so we ought not to fail to get good agreement here. Indeed, all the c_f predictions are correct within the accuracy of the data and there is generally good agreement with the measured values of H_{12}. There are two discrepancies worth noting however. Firstly, at the highest injection rate, Simpson's values of H_{12} fall off towards the end of the plate, a behaviour which agrees neither with the predictions nor with the other experimental data.

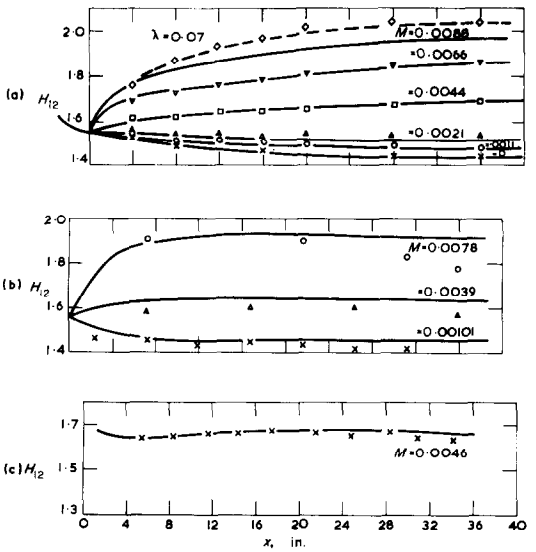

FIG. 2. Predictions of zero pressure gradient air injection H_{12} data of (a) [2] (b) Simpson [22] (c) McQuaid [21].

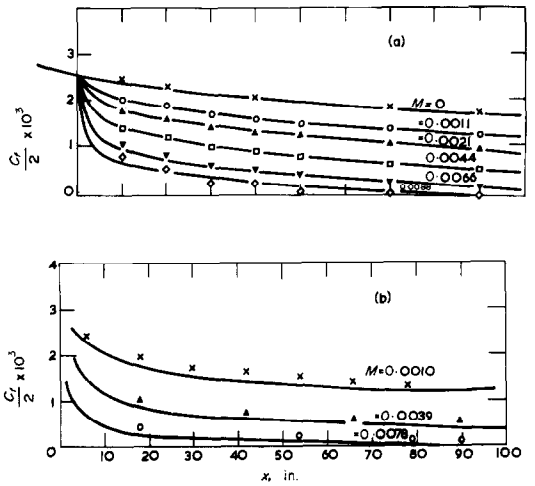

FIG. 3. Predictions of air injection zero pressure gradient of data of (a) [2] (b) Simpson [22].

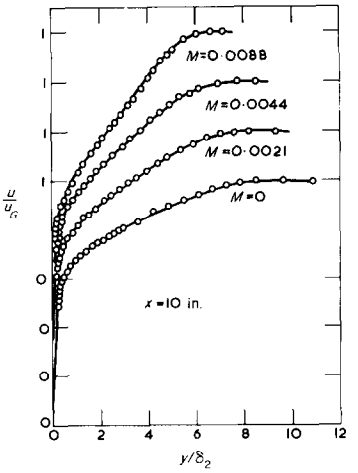

FIG. 4. Predictions of velocity profiles with air injection and zero pressure gradient for [2].

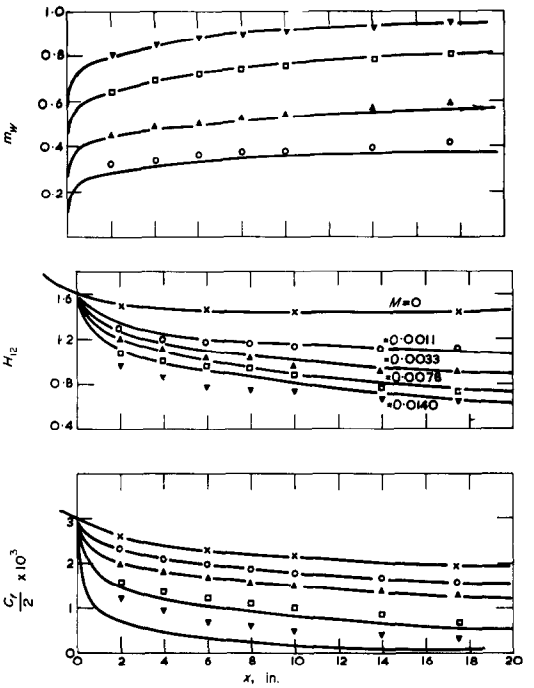

FIG. 5. Predictions of the freon injection data in zero pressure gradient for [2].

Second, predictions of the authors' H_{12} data are about 5 per cent below measurements for $M = 0{\cdot}088$, a behaviour that recurs in other predictions; for reference we show that a reduction of λ to 0·07 brings predictions into agreement with measurements. A selection of predicted and measured velocity profiles are shown in Fig. 4; agreement between the two is virtually complete in both the near-wall and the wake region of the boundary layer.

Prediction of the freon-injection data [1] are shown in Figs. 5 and 6. Because of the introduction of high density gas at the wall the shape factor now *falls* as M is increased. Agreement is satisfactory except the predicted C_f at the highest injection rate; its value is only one third that of the measured. For such a large value of M however, the error could arise from $<0{\cdot}5$ per cent error in measuring δ_2. Since this pattern of disagreement is not repeated in any of the other flows considered we think it likely that the experimental data are in error here. Figure 6 shows the development of the velocity and concentration pro-

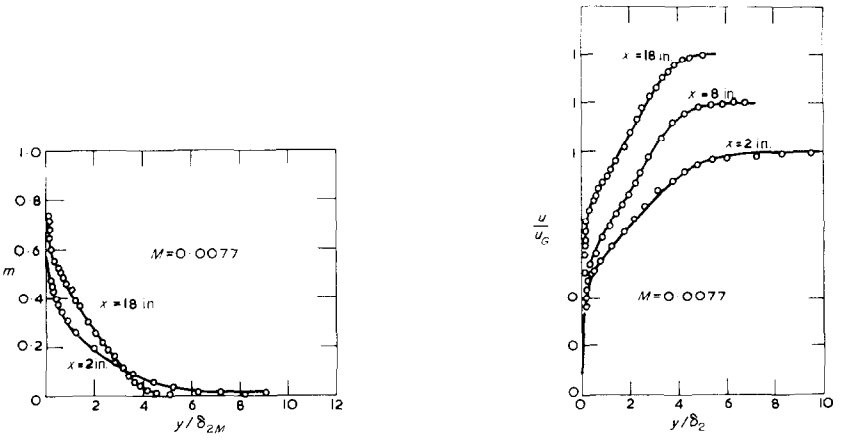

FIG. 6. Predictions of velocity and concentration profiles for freon injection and zero pressure gradient for [2].

files along the plate for $M = 0{\cdot}0077$; again the predicted profiles are almost indistinguishable from a best fit through the data. This indicates how sensitive H_{12} may be to very small differences in velocity distribution; for at $x = 2$ in. there is a significant difference shown in Fig. 5 between measured and predicted values of H_{12}. As the final comparison for zero pressure gradient Fig. 7 compares predicted

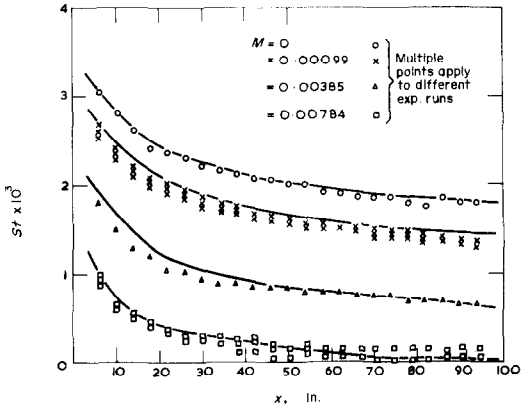

FIG. 7. Comparison of the predictions with the heat-transfer data of Moffat and Kays [23].

Stanton numbers with Moffat and Kays' [23] measurements. Agreement throughout is probably within the accuracy of the data though at the lowest M predictions are about 4 per cent higher than a mean line through the data. The discrepancy would not be worth mentioning were it not that a consistent trend is shown in Fig. 5 for the lowest rate of freon injection.*

* The wall mass fraction is related to the Stanton number by the formula:

$$S_t = M(m_w - 1)/m_w.$$

Measurements and predictions of the present favourable pressure gradient tests are shown in Figs. 8–10 for air and freon injection respectively. A complete tabulation of these and other data is given by Baker [2] and Appendix 2 provides boundary-condition information for use by predictors. In these flows, since v_w is nearly constant over the plate, the parameter M diminishes from the forward to the trailing edge of the porous section as u_G increases. This is why, at the highest injection rate, the shape factor in Fig. 8 rises at first then falls. The acceleration parameter K is fairly uniform with a level of about $1{\cdot}3 \times 10^{-6}$, i.e. about half that required to cause reversion of an untranspired flow to laminar. For both air and freon injection correspondence between measured data and prediction is again very close: both show that the acceleration leads to appreciably higher levels of c_f than when $dp/dx = 0$. As before, the predicted profiles of u and m shown in Fig. 10 are virtually indistinguishable from the experimental data.

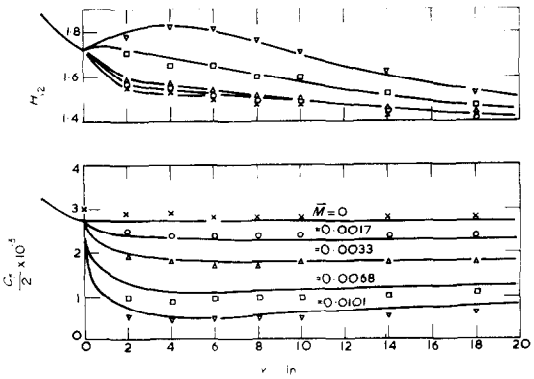

FIG. 8. Predictions of the air injection data in a favourable pressure gradient for [2].

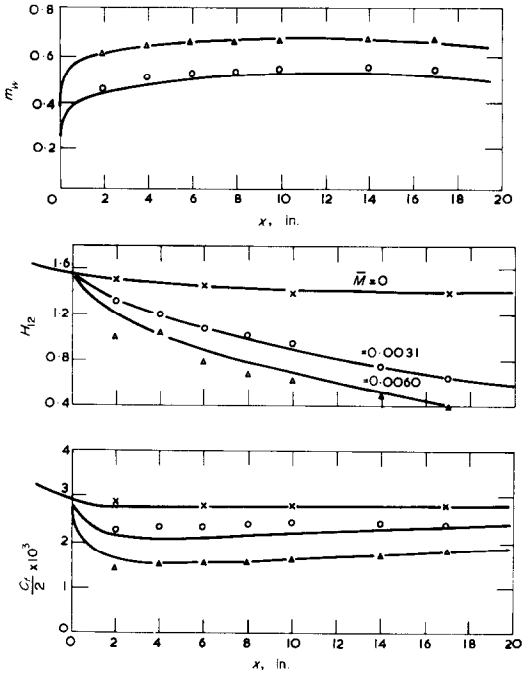

FIG. 9. Predictions of the freon injection data in a favourable pressure gradient for [2].

In McQuaid's [21] favourable pressure gradient test blowing began before the acceleration was applied and continued after it fell off. The shape factor shown in Fig. 11 reflects this sequence by increasing at first, falling for a time and then increasing again towards the end of the plates; the predictions reproduce this behaviour very closely.

Perhaps the most challenging data available of accelerated transpired boundary layers are some of those obtained by Kays' group [24, 25]. Four such tests are shown in Figs. 12 and 13; in all cases step changes in acceleration level are imposed on a con-

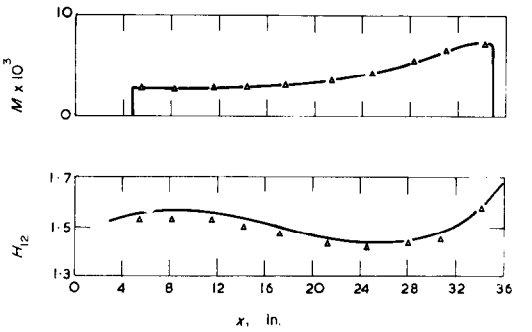

FIG. 11. Comparison of predictions with McQuaids' [21] favourable pressure gradient data.

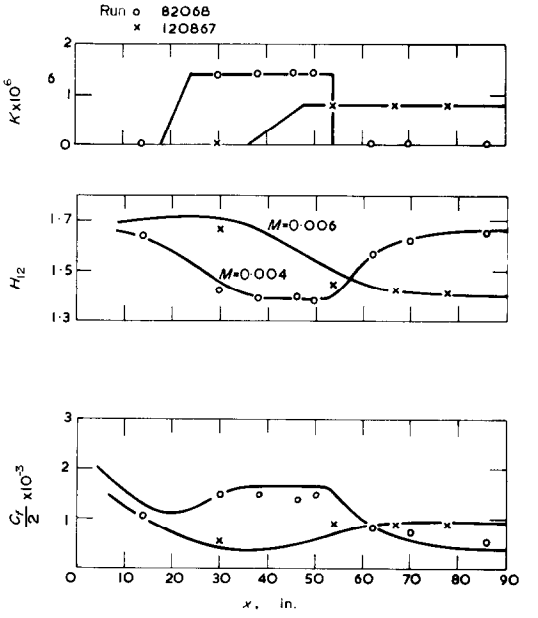

FIG. 12. Comparisons of predictions with Julien's [24] hydrodynamic data in a moderate favourable pressure gradient.

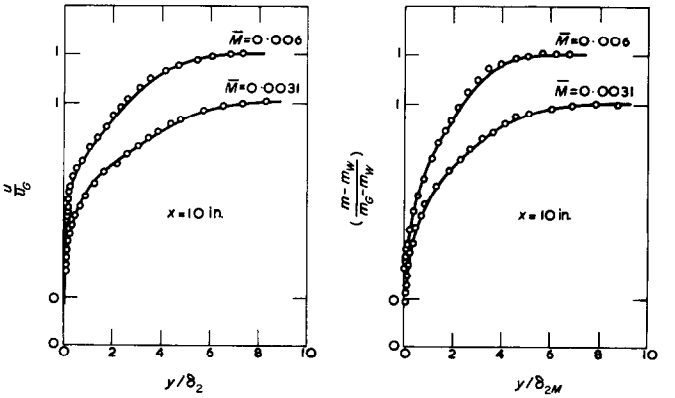

FIG. 10. Predictions of velocity and concentration profiles for freon in a favourable pressure gradient for [2].

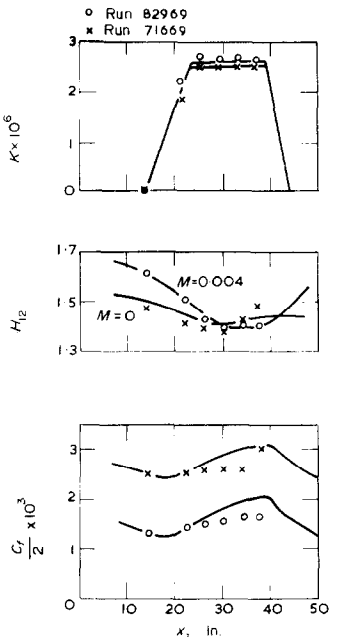

FIG. 13. Comparison of predictions with Loyd's [25] strong favourable pressure gradient.

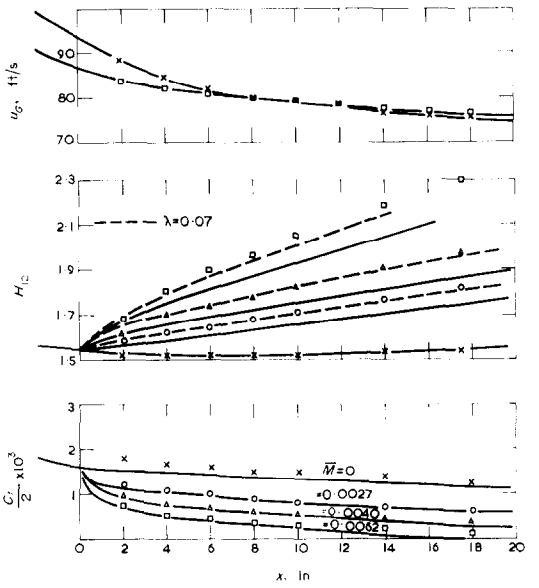

FIG. 14. Predictions of the air injection data in an adverse pressure gradient for [2].

stant-M level of transpiration. In Fig. 12 it is seen that about the correct rate of change of H_{12} and c_f is predicted following the application and removal of dp/dx. The result supports the view that the use of the damping functions of equation (8) enables the 'lag equation' for A^+ to be dispensed with. The flows considered in Fig. 13 are for higher levels of acceleration; predictions are again in generally satisfactory agreement with experiment.

Predictions and measurements of the present data for flow in an adverse pressure gradient with air injection are shown in Fig. 14. Here a mild adverse pressure gradient had been applied from 12 in. upstream of the blown section. For these tests the local level of M increases with distance downstream as U_G falls. It is seen from the H_{12} curves that, for large M, λ needs to be reduced in order to get satisfactory predictions. The only serious discrepancy in c_f occurs at the last measuring station for the highest injection rate. Momentum balance suggested a small positive value of c_f at 18 in. whereas the prediction indicates separation at $x = 16$ in. We think it probable that at 18 in. the flow had just separated since the dynamic pressure recorded by a pitot against the surface was equal to the static pressure there.

The corresponding measurements for freon injection are shown in Fig. 15. The adverse pressure gradient was rather more severe than for the case of air injection. We include the variation of R_2 with x

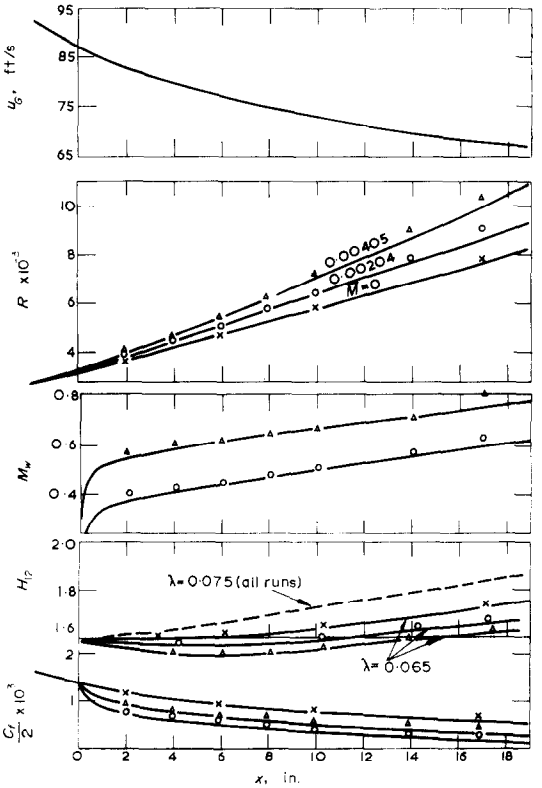

FIG. 15. Predictions of the freon injection data in an adverse pressure gradient for [2].

because this case is the only one where there is any significant disagreement between measurement and prediction. As remarked earlier, because of the insignificant contribution of c_f to the momentum balance in transpired flows, lack of agreement between measured and predicted R_2's is usually a sign that the measured flow is not quite two-dimensional. The problem of obtaining two-dimensional flow is especially severe in an adverse pressure gradient because the rapid thickening of the side-wall boundary layers will cause the flow along the test plate to converge. In most cases, as here, the predicted growth of R_2 is less than measured (for further examples of untranspired flows see Kline *et al.* [26]). Here we see that to obtain reasonable predictions of H_{12} the value of λ must be reduced from 0·075 to 0·065. Sample velocity and concentration profiles are shown in Fig. 16 for the

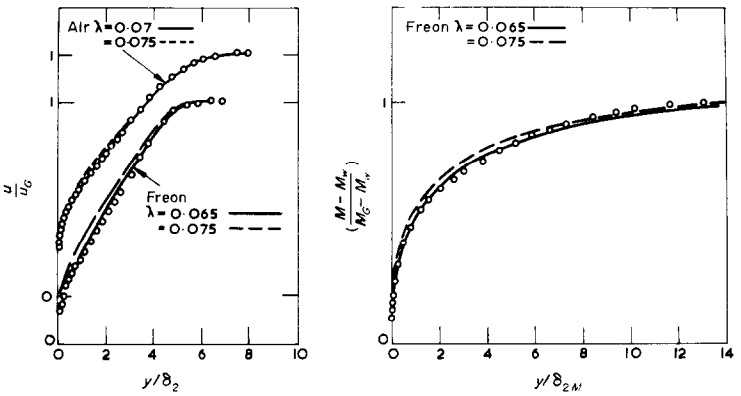

FIG. 16. The influence of different values of λ upon the predictions of the adverse pressure gradient for [2] ($\bar{M} = 0{\cdot}004$ and $x = 10$ in.).

two values of λ; the disagreement between prediction and experiment on these plots does not, perhaps, look so serious here as it does in Fig. 15. As before, c_f and and m_w values shown in Fig. 15, are not greatly affected by the value of λ; agreement of predictions with experiment falls within experimental uncertainty.

The above predictions consistently indicate that adverse pressure gradients or high injection rates cause λ to be smaller than under zero-pressure-gradient conditions with zero or small injection rates. Bradshaw [27] has previously drawn the same conclusion regarding the effect of pressure gradient on mixing length. We believe the cause may be traced to the very rapid thickening of the boundary layer under the conditions in question. By taking the mixing length in the outer part of the boundary layer proportional to y_G we are presuming that the dimensions of the energy containing motions are a function of the *local* boundary layer thickness. But, in fact, these eddies will on average have originated many boundary layer thicknesses upstream and so carry some of the character of the boundary layer at an earlier stage in its development. When the boundary layer undergoes only slow evolution this 'historical' influence is not noticeable for the boundary layer thickness will not change drastically over the lifetime of a typical energy containing eddy. In strongly blown and retarded boundary layers, however, the 'mixing length' of the eddies is really indicative of the flow some distance upstream where the boundary layer was appreciably thinner. Consequently the apparent value of λ falls. To remedy this shortcoming one needs to *calculate* the length scale from its own transport equation rather than prescribe it; this is what the more elaborate 2-equation turbulence models do, e.g. [4].

McQuaid's adverse pressure gradient test is for only a small dp/dx and M. The standard value of λ (0·075) predicts the data well [2] though the test case is not a severe one; for this reason we do not show it. Thompson's [28] data provide interesting cases because dp/dx is severe and separation is prevented only by *suction* through the surface. Of these flows test "H" and the leading 14 in. of test "J" provided both a severe test and a set of data which seemed very closely two-dimensional. For test "H" shown in Fig. 17 the suction velocity approached 1 per cent of u_G keeping R_2 virtually constant along the plate; agreement with the shape factor variation is reasonably good. For test "J", shown in Fig. 18, the pressure gradient is nearly as severe but M is only about $-0{\cdot}004$; R_2 therefore increases downstream. The predicted shape factor falls slowly below the measured values as the flow develops downstream, indicating that here, too, a slightly smaller value of λ would be appropriate.

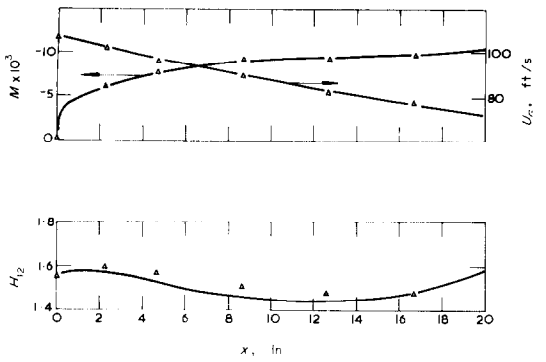

FIG. 17. Comparison of the predictions with Thompsons' [28] suction layer H in an adverse pressure gradient.

The final set of predictions relate to the present experiments in nozzle D (see Fig. 1) where a severe favourable pressure gradient is followed by an adverse one. We have not attempted to deduce an experimental value for c_f in this case because streamwise changes in flow structure are so rapid. We see from Figs. 19–21 however, that for both air and freon injection the agreement between measurement and prediction is quite remarkable: calculated shape factors, wall concentrations and the u and m profiles are all virtually indistinguishable from the data.

The above result at first may seem strange for it appears to conflict with the earlier finding that λ generally needs to be reduced in an adverse pressure gradient. The important difference, in the present case, is that the region of positive dp/dx is preceded by a region of strong acceleration. Through the acceleration the boundary layer decreases in thickness and so, because of the convection effect discussed above, at

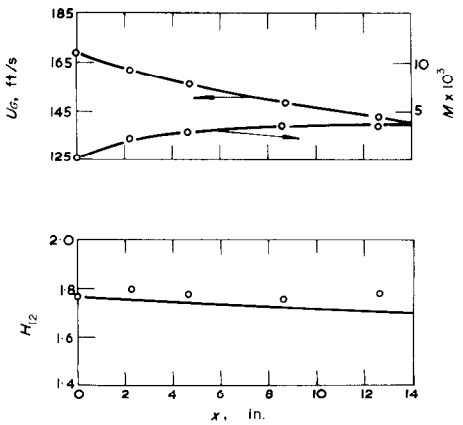

FIG. 18. Comparison of the predictions with Thompson's [28] suction layer J in an adverse pressure gradient.

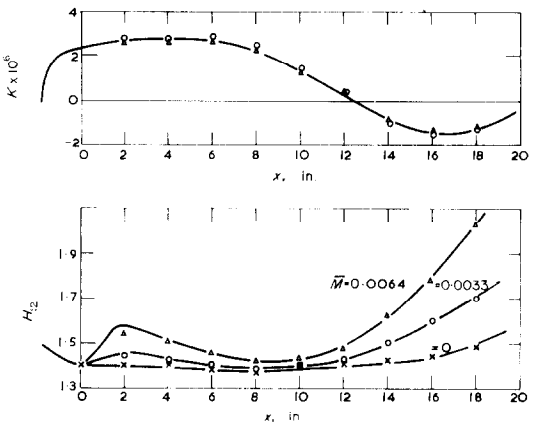

FIG. 19. Predictions of the air injection data for the favourable–adverse pressure gradient for [2].

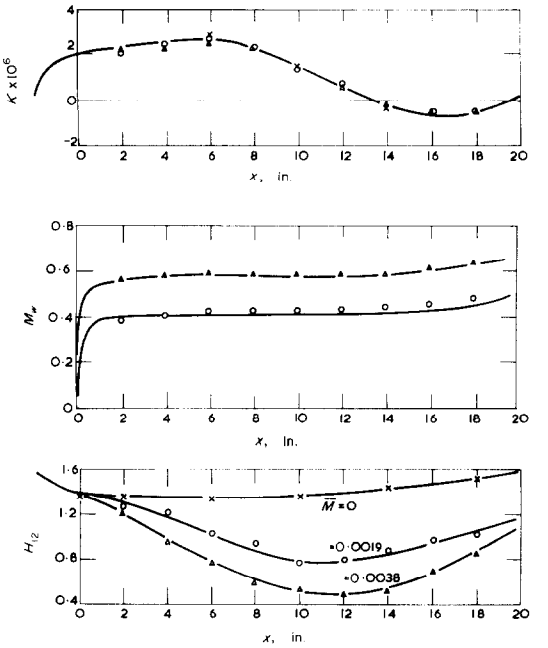

FIG. 20. Predictions of the freon injection data for the favourable–adverse pressure gradient for [2].

the end of the acceleration the mixing length is *larger* than λy_G. Now, in an accelerating flow predictions are not sensitive to the value of the mixing length in the outer half of the layer because the shear stress is low there; that is why accuracy in the accelerated region is not impaired. Moreover, this abnormally large value of λ is carried over into the region of adverse pressure gradient and thus makes

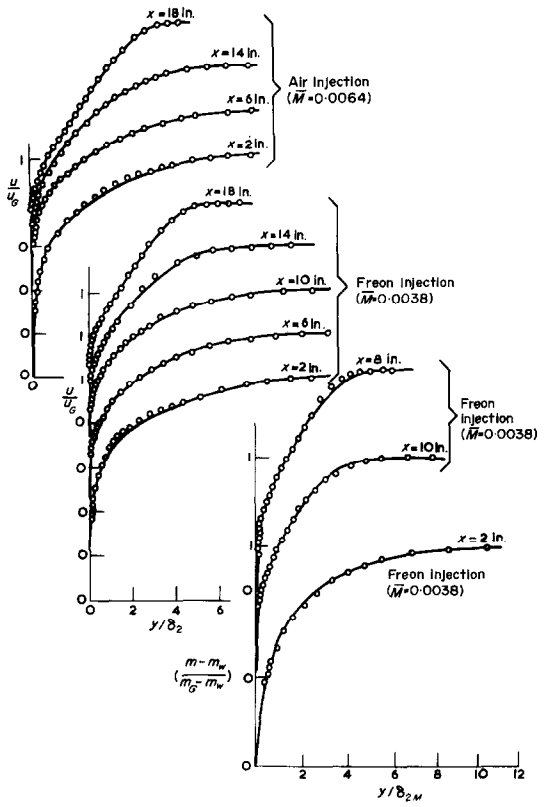

FIG. 21. Predictions of velocity and concentration profiles for the favourable–adverse pressure gradient for [2].

l larger than would have been the case if a zero pressure gradient region had preceded the retardation. It seems that for the above reasons the 'standard value' of λ rather fortuitously gives good predictions throughout.

4. CONCLUDING REMARKS

The paper has proposed a simple version of the mixing length hypothesis for calculating boundary layers on porous surfaces. In the previous section the model has been used to obtain extensive predictions of transpired flow including data from the present study involving strong lateral density gradients and streamwise pressure gradients. The emphasis has been to provide the most searching tests available so that inherent shortcomings of the model as well as its successes, should come to light.

For most of the flows considered the model has acquitted itself very well. We have consistently found, however, that in order to predict accurately flows under high levels of injection ($M \sim 0{\cdot}01$), particularly in adverse pressure gradients, the value of λ needs to be reduced below the standard high-Reynolds-number value of 0·075. In section 4 we argued that the reduction in the 'true' value of λ was due to convective transport under conditions of rapid boundary layer growth. The result suggests that in these extreme flows we should calculate l from a convective transport equation as is done in [4].

Acknowledgements—The research has been generously supported by the Procurement Executive, Ministry of Defence and is published with the Ministry's permission.

Our thanks are also due to Dr. W. P. Jones who provided us with a deck of the Patankar–Spalding program that very nearly matched our needs.

REFERENCES

1. R. J. Baker and B. E. Launder, The turbulent boundary layer with foreign gas injection: I—Measurements in zero pressure gradient, *Int. J. Heat Mass Transfer* **17**, 275 (1974).
2. R. J. Baker, The transpired turbulent boundary layer with streamwise pressure gradient, Ph.D. Thesis, University of London (1971).
3. W. P. Jones and B. E. Launder, The prediction of laminarisation with a 2-equation model of turbulence, *Int. J. Heat Mass Transfer* **15**, 301 (1972).
4. W. P. Jones and B. E. Launder, The prediction of low Reynolds number phenomena with a 2-equation model of turbulence, *Int. J. Heat Mass Transfer* **16**, 1119 (1973).
5. K. Hanjalic and B. E. Launder, A Reynolds stress model of turbulence and its application to thin shear layers, *J. Fluid Mech.* **51**, 609 (1972).
6. T. E. Powell and A. B. Strong, Calculation of the 2-dimensional turbulent boundary layer with mass addition and heat transfer, Proc. 1970 Heat Transfer and Fluid Mech. Inst. (1970).
7. T. Cebici and G. Mosinskis, Prediction of turbulent boundary layers with mass addition including accelerated flows, *J. Heat Transfer* **93**, 271 (1971).
8. W. M. Kays, R. J. Moffat and W. H. Thielbahr, Heat transfer to the highly accelerated turbulent boundary layer with and without mass addition, *J. Heat Transfer* **92**, 499 (1970).
9. W. M. Kays, Heat transfer to the transpired turbulent boundary layer, *Int. J. Heat Mass Transfer* **15**, 1023 (1972).
10. M. P. Escudier, The distribution of mixing length in turbulent flows near walls, Imperial College Mech. Eng. Dept. Rep. TWF/TN/1 (1965).
11. R. Simpson, Characteristics of turbulent boundary layers at low Reynolds numbers with and without mass addition, *J. Fluid Mech.* **42**, 769 (1970).
12. D. E. Coles, The turbulent boundary layer in a compressible fluid, RAND Rep. R-403-PT (1962).
13. E. R. Van Driest, On turbulent flow near a wall, *J. Aero. Sci.* **23**, 1007 (1956).
14 (a) S. V. Patankar and D. B. Spalding, *Heat and Mass Transfer in Boundary Layers*, 1st Edition. Morgan–Grampian, London (1967).
14 (b) *Ibid*, 2nd Edition. Intertext, London (1970).
15. W. P. Jones and B. E. Launder, On the prediction of laminaresant turbulent boundary layers, ASME paper 69-HT-13 (1969).

16. B. E. Launder and W. P. Jones, A note on Bradshaw's hypothesis for laminarization, ASME paper 69-HT-12.
17. P. S. Anderson, W. M. Kays and R. J. Moffat, The turbulent boundary layer on a porous plate: An experimental study of the fluid mechanics for adverse free stream pressure gradients, Thermosciences Division Rep HMT-15, Stanford University (1972).
18. R. L. Simpson, D. G. Whitten and R. J. Moffat, An experimental study of the turbulent Prandtl number of air with injection and suction, *Int. J. Heat Mass Transfer* **13**, 125 (1970).
19. J. Blom, An experimental determination of the turbulent Prandtl number in a developing temperature boundary layer, Thesis, Technische Hogeschool, Eindhoven (1970).
20. J. Rotta, Turbulent boundary layers in incompressible flow, *Progress in Aero. Sci.*, Vol. 2 edited by Ferri, Sterne Küchemann. Macmillan (1962).
21. J. McQuaid, Experiments on incompressible turbulent boundary layers with distributed injection, ARC 28735 (1967).
22. R. L. Simpson, W. M. Kays and R. J. Moffat, The turbulent boundary layer on a porous plate: An experimental study of the fluid dynamics with injection and suction, Thermosciences Division Rep HMT-2, Stanford University (1967).
23. R. J. Moffat and W. M. Kays, The turbulent boundary layer on a porous wall: experimental heat transfer with uniform blowing and suction, Thermosciences Division Rep HMT-1, Stanford University (1967).
24. H. L. Julien, W. M. Kays and R. J. Moffat, The turbulent boundary layer on a porous plate: experimental study of the effects of a favourable pressure gradient, Thermosciences Division Rep HMT-4, Stanford University (1969).
25. R. J. Loyd, R. J. Moffat and W. M. Kays, The turbulent boundary layer on a porous plate: an experimental study of the effects of a favourable pressure gradient, pressure gradient and blowing, Stanford University, Thermoscience Division Rep HMT-13 (1970).
26. S. J. Kline, M. V. Morkovin, G. Sovran and D. J. Cockrell (Eds), Computation of turbulent boundary layers-1968, AFOSR-IFP-Stanford Conference (1968).
27. P. Bradshaw, The response of a constant-pressure turbulent boundary layer to the sudden application of an adverse pressure gradient, ARC R+M No. 3575 (1969).
28. B. G. Thompson, An experimental investigation in the behaviour of the turbulent boundary layer with distributed suction in regions of adverse pressure gradient, ARC R and M 3621 (1970).
29. G. R. Wilke, A viscosity equation for gas mixtures, *J. Chem. Phys.* **18** (1950).
30. J. O. Hirschfelder, C. F. Curtiss and R. B. Bird, *Molecular Theory of Gases and Liquids*. Wiley, New York (1954).

APPENDIX 1

Transport and Other Properties for Freon/Air Mixtures

The molecular viscosity of the gas mixture was obtained from Wilke's [29] relation for a binary gas. For a freon–air mixture, it turned out that this (considerably more elaborate) formula implied that, within very close limits, the kinematic viscosity was a linear function of the mass fraction, i.e.

$$\nu = \nu_F m + \nu_A(1 - m). \tag{A.1}$$

We determined ν from the above equation and obtained the dynamic viscosity by multiplying by the mixture density ρ defined as:

$$\rho = \frac{\rho_A \rho_F}{\rho_F(1 - m) + \rho_A m}. \tag{A.2}$$

Experimental data on the molecular Schmidt number for air–freon mixtures could not be found from any of the usual sources. The manufacturers of Freon provided a calculated value for pure freon of 0·21, and the Lennard–Jones equation (see Hirschfelder *et al.* [30]) indicated values ranging from 0·20 for pure Freon to 1·2 when only a trace was present. We felt uncertain of the accuracy of these analytical estimates and hence turned to concentration measurements of reference [1] to provide an independent estimate. Within the viscous sublayer the species equation, with streamwise convective transport neglected, may be integrated to give

$$\left(\frac{1 - m}{1 - m_w}\right) = \exp\left(\frac{\dot{m}''_w y\, \sigma_m}{\mu}\right) \tag{A.3}$$

which may be converted to the following equation for σ_m

$$\sigma_m = \ln\left(\frac{1 - m}{1 - m_w}\right) \Big/ \frac{\dot{m}''_w y}{\mu}. \tag{A.4}$$

Equation (A.4) is thus used to obtain a value for σ_m from measured values of $\dot{m}''_w$, m_w and of the $m \sim y$ profile in the immediate vicinity of the wall.* The values for σ_m that emerged lent support to the value of 0·2 for pure Freon and displayed a roughly linear variation with m_w. The low-concentration data suggested, however, a value of about 0·7 for $m \to 0$, i.e. rather lower than implied by the Lennard–Jones formula. The result is probably due partly to the fact that the concentration probe was not fully immersed in the viscous sublayer at low injection rates (since τ_w is then larger and, for a given distance from the wall, $y+$ is bigger). We therefore used the following formula giving values intermediate between those obtained from the Lennard–Jones formula and those inferred from experiment:

$$\sigma_m = 0{\cdot}9 - 0{\cdot}7 m_w. \tag{A.5}$$

APPENDIX 2

The following tables give the boundary conditions for predictions of the data. The free stream velocity variation is defined as:

$$u_G = C_0 + C_1 x + C_2 x^2 + \ldots$$

where x is in inches. The mean injection rate is given in terms of $\bar{m}''_w/\rho_G$ to reduce sensitivity of the predictions to small free stream density variations. The local injection rate may be obtained as follows

$$M = \frac{1}{u_G}\left[\frac{\dot{m}''_w}{\rho_G}\right][1 - 0{\cdot}0248\, x + 0{\cdot}00342\, x^2 - 0{\cdot}000101\, x^3].$$

* Equation (A.4) is strictly true only if μ and σ_m are uniform. In practice, however, the small variations in μ and σ_m over the region where (A.4) was fitted do not have a significant effect on the estimated value of σ_m.

Boundary Conditions for Predictions of Present Data and Those of [1]

		$\bar{M} \times 10^3$	$\frac{\bar{m}''_w}{\rho_G}$ (ft/s)	Initial profile at $x = 0$		Free stream velocity (ft/s) $0 < X < 20$ (in.)			$X < 0$
				R_2	H_{12}	$C_0 \times 10^{-1}$	$C_1 \times 10^1$	$C_2 \times 10^3$	$C_0 \times 10^{-1}$
Zero pressure gradient [1]	Air	0	0	520	1·50	9·76	0	0	9.76
		1·09	0·106	480	1·52	9·66	2·23	−8·83	9·66
		2·14	0·209	490	1·49	9·70	0·71	0·30	9·70
		4·41	0·426	480	1·48	9·59	0·69	0·18	9·59
		6·63	0·645	470	1·43	9·57	1·65	−1·35	9·57
		8·83	0·858	500	1·41	9·47	2·63	−0·78	9·47
	Freon	0	0	480	1·65	5·77	0	0	57·7
		1·65	0·095	520	1·64	5·68	0·37	0·11	56·8
		3·34	0·190	650	1·62	5·70	−0·71	4·17	57·0
		7·75	0·436	760	1·70	5·60	0·18	−0·66	56·0
		14·01	0·801	700	1·70	5·68	−0·09	2·19	56·8
Favourable pressure gradient	Air	0	0	320	1·50	3·38	5·48	4·42	3·38
		1·70	0·074	320	1·50	3·42	4·46	4·89	3·42
		3·33	0·147	350	1·52	3·44	4·94	4·62	3·44
		6·75	0·297	300	1·58	3·38	5·29	4·73	3·38
		10·07	0·443	300	1·63	3·37	5·04	4·95	3·37
	Freon	0	0	450	1·56	3·54	5·62	4·55	3·54
		3·06	0·135	560	1·53	3·41	4·87	4·82	3·41
		6·02	0·269	550	1·54	3·82	−0·13	6·43	3·82
Adverse pressure gradient	Air	0	0	1900	1·61	9·13	−11·45	1·18	Adverse p.g. upstream
		2·66	0·213	1800	1·59	8·88	−10·29	1·33	
		4·02	0·321	1750	1·63	8·74	−8·94	1·12	
		6·22	0·494	1650	1·62	8·51	−7·12	1·05	
	Freon	0	0	3250	1·62	8·71	−14·75	2·25	Adverse p.g. upstream
		2·04	0·152	3400	1·62	8·57	−14·56	2·44	
		4·05	0·300	3450	1·62	8·44	−13·05	1·95	

		$\bar{M} \times 10^3$	$\frac{\bar{m}''_w}{\rho_G}$ (ft/s)	Initial profile at $X = 0$		Free stream velocity (ft/s) $-2 < X < 20$ (in.)						$X < -2$
				R_2	H_{12}	$C_0 \times 10^{-1}$	$C_1 \times 10^0$	$C_2 \times 10^2$	$C_3 \times 10^2$	$C_4 \times 10^3$	$C_5 \times 10^4$	$C_6 \times 10^6$	$C_0 \times 10^{-7}$
Favourable Adverse	Air	0	0	860	1·54	4·33	1·23	−2·76	9·75	−9·26	2·23	0·08	3·97
		3·25	0·228	860	1·54	4·28	1·09	3·03	10·75	−12·08	4·04	−3·46	3·97
		6·40	0·439	860	1·54	4·12	0·99	24·73	4·98	−6·70	1·97	−0·65	3·97
	Freon	0	0	1000	1·44	4·01	0·90	42·13	2·12	−4·43	1·08	0·62	3·97
		1·92	0·133	1000	1·44	4·54	0·16	−55·06	3·87	−34·48	14·60	−21·57	3·97
		3·84	0·266	1000	1·44	4·17	0·96	15·51	7·17	−8·15	2·21	−0·40	3·97

COUCHE LIMITE TURBULENTE AVEC INJECTION DE GAZ ETRANGER: II—CALCUL ET MESURE DANS DE SEVERES GRADIENTS DE PRESSION LONGITUDINAUX

Résumé—L'article propose une version nouvelle et simple de la longueur de mélange de Prandtl pour un écoulement le long de surface lisses. Le modèle a été utilisé pour obtenir une extension aux couches limites sur des surfaces poreuses, incluant des écoulements avec des gradients élevés de densité et de température, mesurés dans cette étude. Un très bon accord des calculs et des mesures est obtenu sauf dans des écoulements à gradient de pression adverse et sous des conditions de soufflage intense. Dans ces cas, à cause du transport convectif de turbulence, la valeur de la longueur de mélange dans la zone externe de la couche limite ne croît pas aussi rapidement que l'épaisseur de la couche limite.

DIE TURBULENTE GRENZSCHICHT MIT FREMDGASEINSPRITZUNG—II. BERECHNUNGEN UND MESSUNGEN BEI STARKEN DRUCKGRADIENTEN

Zusammenfassung—Es wird eine neue und einfache Version der Prandtl'schen Mischlängenhypothese für eine Strömung über glatte Oberflächen vorgeschlagen. Dieses Modell wurde zur Bestimmung von Grenzschichten an porösen Oberflächen bei Strömungen mit hohen Dichte- und Druckgradienten herangezogen, wie man Sie in der vorliegenden Arbeit gemessen hat. Die Voraussagen stimmen mit den Messungen sehr gut überein, ausser in Strömungen mit gegenläufigen Druckgradienten und unter der Bedingung starken Einblasens. In diesen Fällen wächst wegen des konvektiven Turbulenztransportes die Mischlänge im äusseren Teil der Grenzschicht nicht so schnell an wie die Dicke der Grenzschicht.

ТУРБУЛЕНТНЫЙ ПОГРАНИЧНЫЙ СЛОЙ С ВДУВОМ ЧУЖЕРОДНОГО ГАЗА: II—РАСЧЕТ И ИЗМЕРЕНИЯ ПРИ ГРАДИЕНТАХ ДАВЛЕНИЯ, НАПРАВЛЕННЫХ СТРОГО ПО ТЕЧЕНИЮ

Аннотация—Предлагается новый и простой вариант гипотезы о длине пути смешения Прандтля при обтекании гладких поверхностей. Модель использовалась для получения подробных расчетов пограничных слоев на пористых поверхностях при течении с резкими градиентами давления и плотности, измеренными в данной работе. В работе представлены также экспериментальные исследования по данному вопросу. Получено очень хорошее соответствие между расчетами и измерениями за исключением случая течений с положительными градиентами давления и сильным вдувом. В этих случаях из-за конвективного турбулентного переноса величина пути смешения на внешней границе пограничного слоя возрастает медленнее по сравнению с толщиной пограничного слоя.